Geomechanics and Engineering, *Vol. 42, No. 1 (2025) 31-42*
https://doi.org/10.12989/gae.2025.42.1.031

Characteristics of void distribution in caving zone and their impact on gangue slurry diffusion properties

Jiaqi Wang*[1], Rui Gao[1a], Meng Li[2b] and Ming Chang[1c]

[1]*College of Mining Engineering, Taiyuan University of Technology, Shanxi 030024, China*
[2]*State Key Laboratory of Coal Resources and Safe Mining, China University of Mining and Technology, Xuzhou, 221116, China*

(*Received October 8, 2024, Revised March 5, 2025, Accepted June 24, 2025*)

Abstract. High gangue emission has emerged as a significant issue impacting the ecological environment in mining areas. Utilizing gangue as an aggregate material to prepare gangue slurry for filling caving zones has gained popularity as a solution. However, due to the intricate nature of coal mine caving zones, the diffusion mechanism of gangue slurry is highly complex, necessitating the elucidation of its diffusion laws to effectively guide mine-filling practices. In this paper, we conducted an analysis of the impact of lithology, skeleton particle gradation, and axial stress on the distribution characteristics of the caving zone, leveraging the internal void evolution test system of mining rock mass and the simulation approach for skeleton particles of fractured rock mass. Furthermore, we established a fluid force balance model to investigate the diffusion characteristics of gangue slurry within the void. As the lithology hardens, the coarse particle size within the skeleton particle grading increases. Consequently, the void rate within the caving zone gradually expands, the void fractal dimension becomes increasingly prominent, and the diffusion depth of gangue slurry gradually intensifies. Lithology serves as the primary factor influencing gangue slurry diffusion. When the lithology hardens, the void ratio increases by 0.26, the void fractal dimension rises to 0.13, and the gangue slurry diffusion depth expands by 208 meters. An industrial practice of gangue grouting has been implemented. The results of on-site monitoring indicate that the diffusion range of gangue slurry aligns with the aforementioned findings, thereby effectively addressing the challenges associated with gangue disposal.

Keywords: caving zone void ratio; diffusion law; gangue slurry; grout filling; lithology

1. Introduction

Coal resources are the primary energy source in China, and a large amount of gangue will be produced in the process of high-intensity mining of coal resources, and its emission accounts for about 10%~15% of coal production (Zhang *et al.* 2016, Li *et al.* 2021, Zhang *et al.* 2018). According to statistics, China's current cumulative gangue production of about 4.5 billion tons and 400-800 million tons of emissions increased year by year (Xue *et al.* 2024, Yoon *et al.* 2024, Lou *et al.* 2024). Gangue discharge is not only a waste of land resources but also prone to gangue mountain spontaneous combustion, the release of toxic and harmful gases that pollute the air environment, heavy metal elements in the gangue by rainwater leaching and surface water, groundwater long-term soaking release, the soil, water environment causing ecological threats, and may be harmful to human health through the way of bioaccumulation (Prendes *et al.* 2013, Mohammadi *et al.* 2018, Kamran *et al.* 2022). Therefore, it is urgent to prevent and control the environmental pollution of coal gangue effectively, and the research on the disposal and utilization of gangue has always been of great concern to scholars.

At present, the harmless utilization of gangue mainly focuses on mine filling and other aspects (Genis *et al.* 2018, Junker *et al.* 2013, Gholizadeh *et al.* 2015). China supports efficient and low-cost gangue filling and replacement technology to expand the source of mine filling materials, among which gangue slurry material is one of the research hotspots (Van Dyke *et al.* 2018, Li *et al.* 2020, Liu *et al.* 2019). Gangue slurry is a low-cost, green, and clean filling material. A large number of scholars at home and abroad have conducted research on gangue slurry filling with large-size gangue as aggregate, which can be adapted to high-concentration and long-distance transportation (Yin *et al.* 2017, Behera *et al.* 2020, Ghazifard *et al.* 2016). After a large number of experimental research and optimization, gangue slurry contains a specific particle size of coarse aggregate, cementing materials, and water, of which the coarse aggregate size is not greater than 15 mm; cementing materials generally use fly ash, the concentration is maintained at 70 ~ 80%. Scholars (Kostecki *et al.* 2015, Hejmanowski *et al.* 2015, Roy *et al.* 2023) research results further show that gangue slurry belongs to the power law fluid by adjusting the gangue slurry concentration and cementing material mass ratio can be designed gangue slurry transportation characteristics and solidification characteristics to achieve the transportation and bearing needs. At present, gangue slurry has been widely used in metal mines and coal mines. The current utilization of

*Corresponding author, Ph,D.
E-mail: wangjiaqi@tyut.edu.cn
[a]Professor
[b]Professor
[c]Ph,D.

ISSN: 2005-307X (Print), 2092-6219 (Online)

Table 1 Usage of gangue slurry

No.	Mine location	Filling position	Filling capacity	Filling material	Pressure
1	Erdos	separation layer	120 t/h	0~10 mm gangue+water	0.5~2 MPa
2	Yulin	striped goaf	250 m^3/h	0~10 mm gangue+water+fly ash	1 MPa
3	Yanan	caving zone	120 t/h	cement+ water+fly ash	1.5 MPa
4	Weinan	caving zone	120 t/h	0~10 mm gangue+water	1.2 MPa
5	Jinzhong	caving zone	150 t/h	0~10 mm gangue+water	0.9 MPa
6	Jinjie	caving zone	120 t/h	ash+water	-

gangue slurry filling in coal mines is shown in Table 1 (Kim *et al.* 2016, Feng *et al.* 2024, Wesseloo *et al.* 2018).

There exists a large amount of space in the caving zone of a coal mine, which is the best location for gangue slurry filling. Related studies show that the void size of the caving zone is closely related to the lithology of overburdened rock, the degree of fracture block of the roof, and the pressure of overburdened rock (Mondal *et al.* 2017, Mo *et al.* 2018, Singh *et al*. 2010). The harder the overburden rock, the larger the fracture block size of the overburden rock, and the longer the non-recombining edge length in the stacking process of the broken roof, the larger the size of the caving zone void; the larger size of the broken rock blocks occlude each other to form the skeleton of the broken rock blocks, which provides stable space for the existence of the void; with the gradual increase of the overburden rock pressure, the caving zone void will be gradually closed. As the size and distribution of the gap in the caving zone are affected by external factors, in order to maximize the use of gangue slurry scientifically, it is necessary to investigate the evolution of the gap in the caving zone and the mechanism and law of gangue slurry diffusion.

However, most of the current research on the gangue slurry diffusion mechanism is mainly applied to the field of metal mines for the single-hole grouting diffusion or the slurry flow law inside the pipeline (Sharma *et al*. 2011, Song *et al.* 2006; Verma *et al.* 2016). Compared with metal mines, the influence factors of void distribution in the coal mine caving zone are more complex, and the forms of voids are mostly interdependent and of different sizes, so it is more difficult to investigate the diffusion law of gangue slurry in this cross-scale porous media space.

To address the aforementioned issues, this article employs a comprehensive approach encompassing laboratory experiments, theoretical analysis, and on-site demonstrations. This integrated framework is utilized to delve into the lithological characteristics, particle size distribution of the broken rock block skeleton, and the distribution patterns of voids within the caving zone under axial stress, along with the diffusion behavior of gangue slurry. A dedicated test system is designed to simulate the evolution of voids in the caving zone, facilitating the analysis of the evolution patterns of both the skeleton particle size distribution and void ratio in various lithological roof types before and after pressure crushing. Furthermore, the diffusion depth of gangue slurry within the cross-scale porous medium space of the caving zone is calculated. To validate the research findings, a practical case study is conducted, drawing upon the grouting filling practices in a mine located in Inner Mongolia. The objective of this comprehensive research is to establish a solid theoretical foundation for the effective application of gangue slurry in grouting operations.

2. Materials, methods, and scheme

2.1 Sources and properties of specimens

Using the method of simulating the skeleton particles of the crushed rock mass in the roof after mining, particles with a size ranging from 10 to 50 mm were chosen as the skeleton particles. Directly sourced from the coal mine, four representative lithologies - limestone, sandstone, mudstone, and shale - were utilized to mimic the crushed rock blocks of varying lithologies within the caving zone. Before the test, the gangue of various lithologies should be crushed to a particle size of less than 50 mm and subsequently screened using grading sieves of 10 mm, 15 mm, 20 mm, 25 mm, 30 mm, 40 mm, and 50 mm.

The preparation of experimental samples rigorously adheres to the principle of equivalence with in-situ surrounding rock characteristics, ensuring the representativeness of pore features through a three-phase process. Initially, four typical roof rock samples-limestone, sandstone, mudstone, and shale-are collected from in-situ mines, preserving their original mechanical properties. Subsequently, these rock samples are processed into characteristic particle sizes ranging from 10 to 50 mm using a controllable crushing technique, and the skeleton particle grading is reconstructed through a precision grading sieve with six classifications within the 10-50 mm range, based on the Talbot index theory (n=0.3-0.6). Lastly, an axial loading system (5-20 MPa) is employed to simulate the stress environment of overlying strata under varying mining depths. This preparation method achieves quantitative equivalent characterization of pore structures between laboratory samples and the in-situ collapse zone through systematic control of lithology, grading, and stress.

The gradation of skeletal particles across six size ranges-10~15 mm, 15~20 mm, 20~25 mm, 25~30 mm, 30~40 mm, and 40~50 mm-was tallied, and the histograms depicting the distribution of skeletal particle gradation for specimens of varying lithologies are presented in Fig. 1.

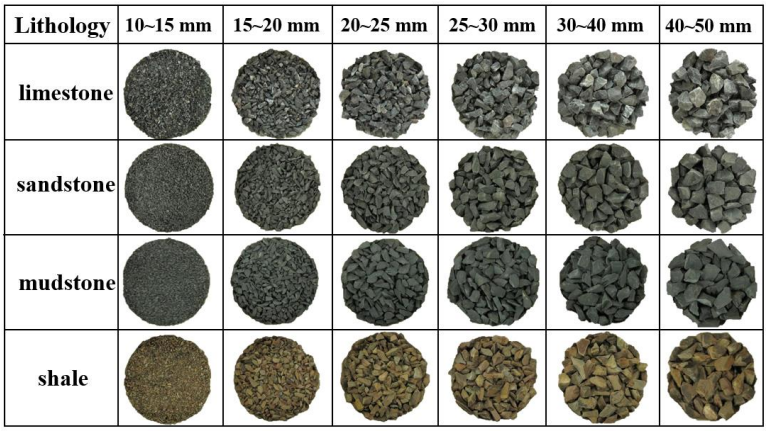

(a) Specimens

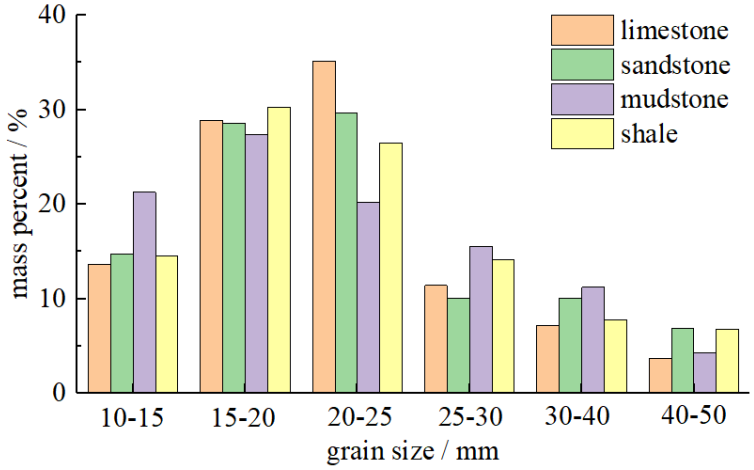

(b) Gradation

Fig. 1 Specimens and gradation of different lithologies

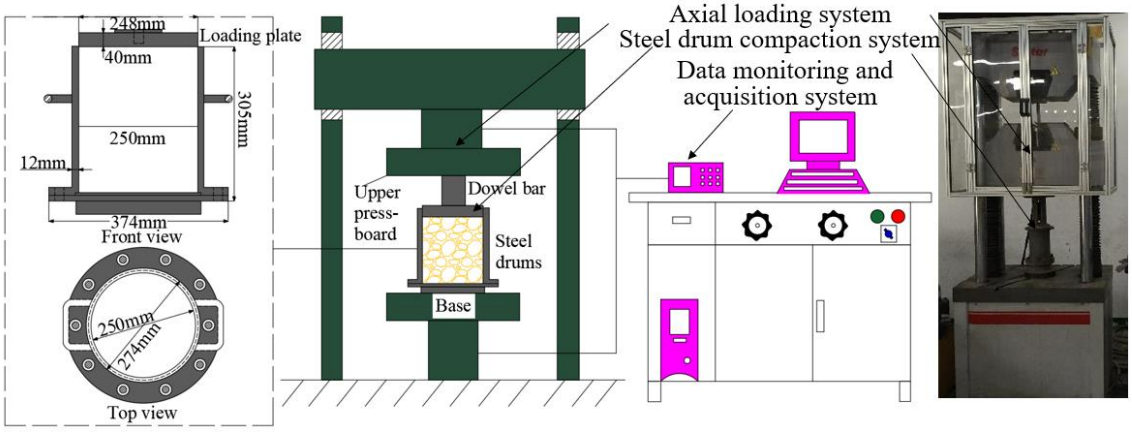

Fig. 2 Systematic diagram of the internal void evolution test system for mining rock blocks

2.2 Test equipment and test methods

(1) Test system

After the extraction of the coal seam, the overlying rock strata undergo breakage and collapse, enduring the pressure of the overlying strata. Analysis of the fractured rock blocks reveals that their sides are constrained by displacement from the coal body, their bottoms are constrained by displacement from the floor, and their tops are subjected to axial stress from the overlying strata. Based on this analysis, the entire internal void evolution test system for mining rock blocks has been designed, comprising three components: an axial loading system, a loading steel drum, and a data monitoring and acquisition system, as shown in Fig. 2.

The WAW-1000D electro-hydraulic servo universal testing machine is employed within the axial loading system of the internal void evolution test for mining rock blocks,

serving to provide consistent and stable axial stress to the fractured rock blocks. The loading steel barrel measures 274 mm in outer diameter, 12 mm in wall thickness, and 305 mm in depth. The data monitoring and acquisition system comprises a load sensor and a travel sensor, enabling the measurement of compaction loads and deformation during the compaction process of the fractured rock. During the experimental process, the displacement loading method is employed to regulate the deformation of the specimen, with a loading rate of 0.01mm/s.

The stress exerted by the overlying strata on the coal seam is calculated based on the overburden density and burial depth. In this study, a burial depth of 660 m corresponds to a vertical stress of approximately 16.5 MPa (assuming an average density of 2.5 g/cm³). During the experiment, the WAW-1000D electro-hydraulic servo testing machine was utilized to apply axial stresses ranging from 5 to 20 MPa (spanning 0.3 to 1.2 times the vertical stress ratio) to the crushed rock samples. The stress levels were monitored in real-time via a load sensor to simulate the effects of overburden pressure at varying mining depths.

(2) Caving zone void parameters

The axial load and axial compression deformation of the sample can be acquired through the data monitoring and acquisition system. By integrating the stress area and loading height of the sample, the void fraction of the sample can ultimately be calculated, as illustrated in formula (1).

$$\varphi = \frac{V_c - V_0}{V_c} = 1 - \frac{m_0}{\rho_0 A(h_0 - \Delta h)} \tag{1}$$

Where, m_0 and ρ_0 represent the mass and density of the sample respectively, while the area subject to force is given by $A = \Pi D^2/4$.

Simultaneously, based on the Tyler fractal theory (Mishra *et al.* 2021), the mass data of each particle group before and after compression can be processed to generate data points plotted with $\lg(d_i/d_{\max})$ as the abscissa and $\lg(M_{l(di)}/M_t)$ as the ordinate. These data points can then be fitted into a "$\lg(d_i/d_{\max})$ - $\lg(M_{l(di)}/M_t)$" curve to calculate the fractal dimension D of the broken rock blocks. This fractal dimension serves as a quantitative indicator of the crushing characteristics of the samples within the space, effectively simulating the roof crushing conditions on site. Within the three-dimensional space of the steel barrel, the fractal dimension of the void distribution is represented by 3-D, as outlined in Eq. (2).

$$3\text{-}D = k \tag{2}$$

Where k is the slope of the " $\lg(d_i/d_{max})$ - $\lg(M_{l(di)}/M_t)$" curve and the void fractal dimension.

From this analysis, it can be seen that the void fractal dimension is related to the grain size and mass share of the specimen, and the smaller the D value is, the worse the crushing effect of the specimen is. The larger the void ratio inside the crushed rock mass is, the larger the k value is.

Analysis reveals that the fractal dimension of voids is correlated with the particle size and mass proportion of the sample. A smaller D value indicates poorer crushing efficiency, resulting in a higher void fraction within the fractured rock block and a correspondingly larger k value.

2.3 Test program

Based on the analysis of the experimental principles, the distribution of voids is influenced by various factors, including the lithology of the sample, the gradation of skeleton particles, and axial stress. Consequently, this paper incorporates the aforementioned internal void evolution test system to investigate the impact of these three primary controlling factors - lithology, skeleton particle size distribution, and axial stress - on both the void fraction and the fractal dimension of void distribution through a series of single-factor rotation experiments.

The rationale behind selecting the three parameters—lithology, skeleton particle grading, and axial stress—is as follows: Lithology dictates the initial structural strength of crushed rock fragments, with harder lithologies resulting in larger fragment sizes and higher porosity upon crushing. Skeleton particle grading influences void connectivity, with an increase in coarse particle proportion leading to an elevation in porosity. Axial stress reflects the compaction effect of the overlying rock, with a lesser decrease in porosity observed under lower stress conditions. By conducting quantitative analysis of these three parameters through laboratory single-factor rotation experiments, we can identify the core variables influencing engineering design, thereby significantly enhancing slurry diffusion depth.

In this study, we utilize rock fragments ranging from 10 to 50 mm in size to simulate the fractured roof of the caving zone, with a geometric similarity ratio of 1:20. By adjusting the Talbot index to replicate the grading curve, we ensure that the porosity of the model aligns with the sub-intervals of the actual caving zone.

During the experiment, the lithology of the samples selected includes sandstone, limestone, mudstone, and shale. The proportion of particle size for each lithology is determined using the Taibo theory, with the Taibo index n set to 0.3, 0.4, 0.5, and 0.6. The specific calculation method is outlined in formula (3).

$$P_i = 100\ (d_i/d_{max})\ \text{^n} \tag{3}$$

Where, P_i represents the passing rate for a specific particle size level; d_i stands for a particular particle size level; d_{max} indicates the maximum particle size within the sample; and n denotes the Tebble index, where a higher value of n within the sample indicates a greater proportion of large-sized particles.

The design axial compressive stresses were 5, 10, 15, and 20 MPa, and the loading rate was 1 kN/s. The test program was designed for a total of 1,000 s, and the data were collected every 3.0 s. The test program is shown in Table 3.

The design axial compressive stresses were set at 5, 10, 15, and 20 MPa, with a loading rate of 1 kN/s. The test program was designed to run for a total duration of 1,000 seconds, and data were collected at an interval of 3.0 seconds. The test schemes are outlined in Table 2.

Table 2 Test schemes table

Number	lithology	Tebble index	axial stress /MPa
T-1	sandstone	n=0.5	15
T-2	limestone		
T-3	mudstone		
T-4	shale		
T-5	sandstone	n=0.3	15
T-6		n=0.4	
T-7		n=0.5	
T-8		n=0.6	
T-9	sandstone	n=0.5	5
T-10			10
T-11			15
T-12			20

Tests T-1 to T-4 were conducted to investigate the impact of lithology on void fraction and void fractal dimension. Similarly, Tests T-5 to T-8 were designed to assess the influence of skeletal particle gradation on void fraction and void fractal dimension. Lastly, Tests T-9 to T-12 aimed to analyze the effect of axial stress on void fraction and void fractal dimension.

The fractal dimension of fragmented rock masses serves as a quantitative indicator of the complexity of the internal void structure within the caving zone. Variations in this dimension directly mirror the geometric features of void distribution under the influence of lithology, grading, and stress, as well as its impact on slurry dispersion. The space of the caving zone can be perceived as a natural porous medium. Given that the ratio between the largest and smallest void sizes within the caving zone surpasses 100 to 1000, it exhibits fractal characteristics of statistical self-similarity in both two-dimensional and three-dimensional directions, aligning with the fractal scaling law. Consequently, the fractal theory of porous media can be employed to investigate the void characteristics of the caving zone.

3. Results

3.1 Evolutionary law of void fraction

The laws governing lithology, skeletal particle gradation, and axial stress, which influence the void ratio of the crushed rock mass, were derived individually and are presented in Fig. 3.

(1) According to the analysis presented in Fig. 3(a), the impact of lithology on void fraction is primarily manifested in the degree of fragmentation. Specifically, harder lithologies result in larger fragments of broken rock samples, leading to larger voids formed by the stacking of these fragments. Consequently, harder lithologies exhibit higher initial void fraction values. For instance, when comparing limestone, sandstone, mudstone, and shale, the initial void fraction of their respective broken rock samples is observed to be 0.42, 0.41, 0.39, and 0.32.

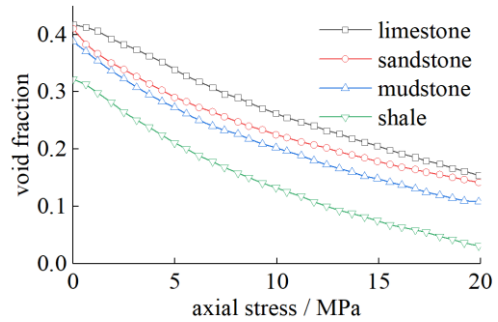

(a) Lithology

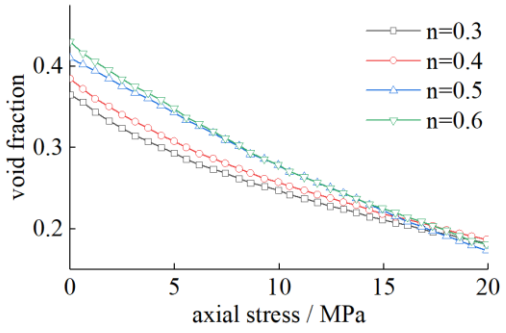

(b) Skeleton particle gradation

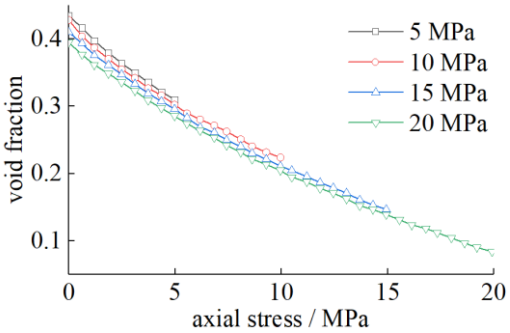

(c) Axial stress

Fig. 3 Evolution pattern of void ratio under the influence of different factors

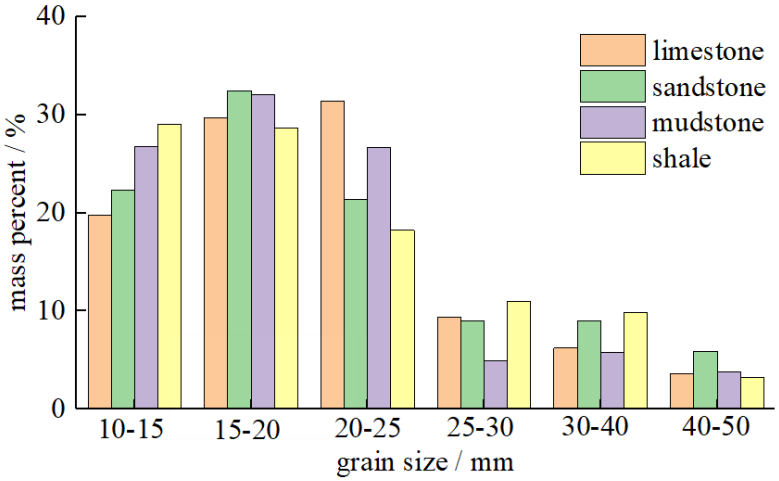

Fig. 4 Distribution of skeletal particle size from different lithology after compression

Upon the application of compressive loads, samples with higher lithological strength exhibit a relatively smaller decrease in void fraction. For instance, the void fraction of broken limestone decreases from 0.42 to 0.16, representing a decrease of 0.26. In contrast, the void fraction of broken sandstone, mudstone, and shale decreases by 0.27, 0.29, and 0.30, respectively. This discrepancy can be attributed to the fact that broken limestone particles possess a stronger resistance to crushing, sliding, and rotation compared to broken shale particles, which are more susceptible to these processes.

(2) Analysis of Fig. 3(b) reveals that the impact of skeleton particle gradation on the void fraction of the caving zone is evident in the fact that a higher proportion of larger particles results in larger void sizes and consequently, a higher void fraction. The larger the particle size of the skeleton particles, the higher the initial void fraction. As the Tebble coefficient n increases, the initial void fraction of the broken rock block varies, specifically, it is 0.37, 0.38, 0.41, and 0.43, respectively.

However, samples with a higher proportion of small particles exhibit a relatively minor decrease in void fraction. For instance, when n=0.3, the void fraction of the sample decreases from 0.36 to 0.18, representing a drop of 0.18. In contrast, when n=0.4, n=0.5, and n=0.6, the void fraction of the sample decreases by 0.20, 0.24, and 0.25, respectively. This is attributed to the fact that, at n=0.3, a significant number of voids are filled with small particles, resulting in a relatively low initial void fraction. Consequently, with the increase of axial stress, there is limited room for further reduction in void fraction.

(3) As depicted in Fig. 3(c), as the axial stress increases, the void fraction gradually decreases, accompanied by a growing decrease amplitude. Precisely, when the axial stress attains 5, 10, 15, and 20 MPa, the corresponding decrease amplitude of void fraction is 0.12, 0.12, 0.11, and 0.10, respectively.

In summary, the lithology and skeleton particle grading of fractured rock blocks are crucial factors determining their initial void fraction. Rock samples with harder lithology and larger skeleton particles are likely to exhibit a higher initial void fraction. When subjected to axial loading, samples with harder lithology and smaller skeleton particle sizes tend to demonstrate a relatively smaller decrease amplitude in void fraction.

3.2 Void fractal dimension evolution laws

After compaction, the graded sieve is utilized to further screen the compacted sample, and the skeleton particle size distribution is recorded both before and after compaction.

The statistical results are presented in Fig. 4.

A comparative analysis of Figs. 1 and 4 reveals that upon compression and crushing, the proportion of small-sized particles in each lithological sample increases significantly, while the proportion of medium-sized particles decreases significantly. Large-sized particles, serving as the skeletal structure, undergo less crushing. Notably, particles with diameters ranging from 20 to 30 mm constitute the primary consumption group, experiencing a 30.8% decrease in mass proportion after crushing. Conversely, particles with diameters between 10 and 15 mm represent the primary group for particle size increase, experiencing a 33.9% increase in mass proportion following crushing.

Ultimately, the fractal dimension of the voids in each group of samples can be derived through computations based on Eqs. (2) and (3), as depicted in Fig. 5.

It can be inferred from Fig. 5 that as the lithology becomes increasingly harder, the fractal dimension of voids within broken rock samples gradually rises, accompanied by an increase in both the number and size of voids. Specifically, when the lithology of the rock samples comprises limestone, sandstone, mudstone, and shale, the fractal dimensions of the voids are observed to be 0.5753, 0.5093, 0.4948, and 0.4476, respectively. Furthermore, as the number of coarse particles in the rock samples increases, the fractal dimension of voids also exhibits a gradual increase, along with an augmentation in the number and size of voids. For instance, when the value of n is 0.3, 0.4, 0.5, and 0.6, the corresponding fractal dimensions of voids are 0.3484, 0.3690, 0.4146, and 0.4447, respectively.

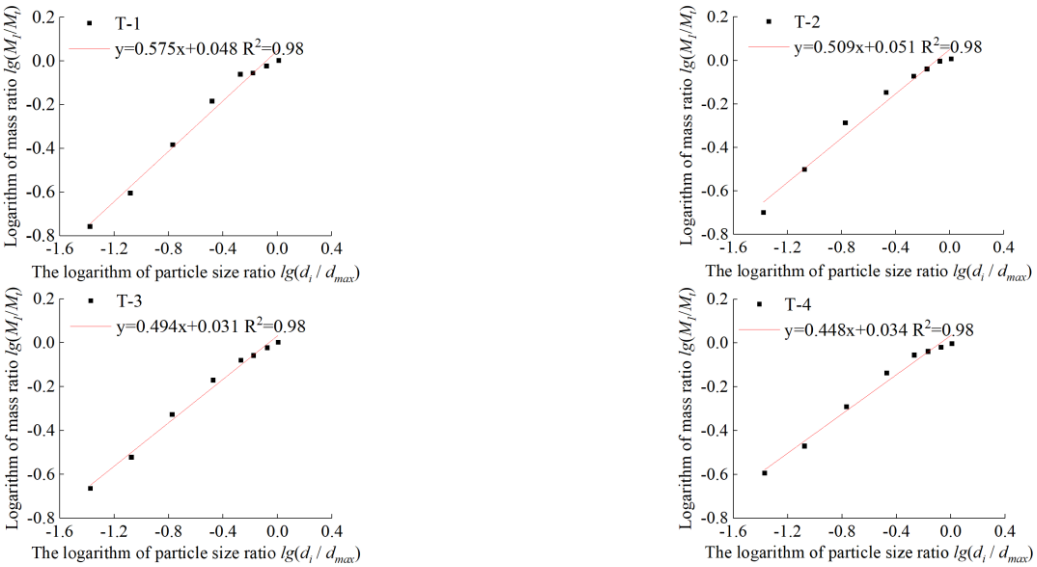

(a) Fractal dimension of voids under the influence of lithology

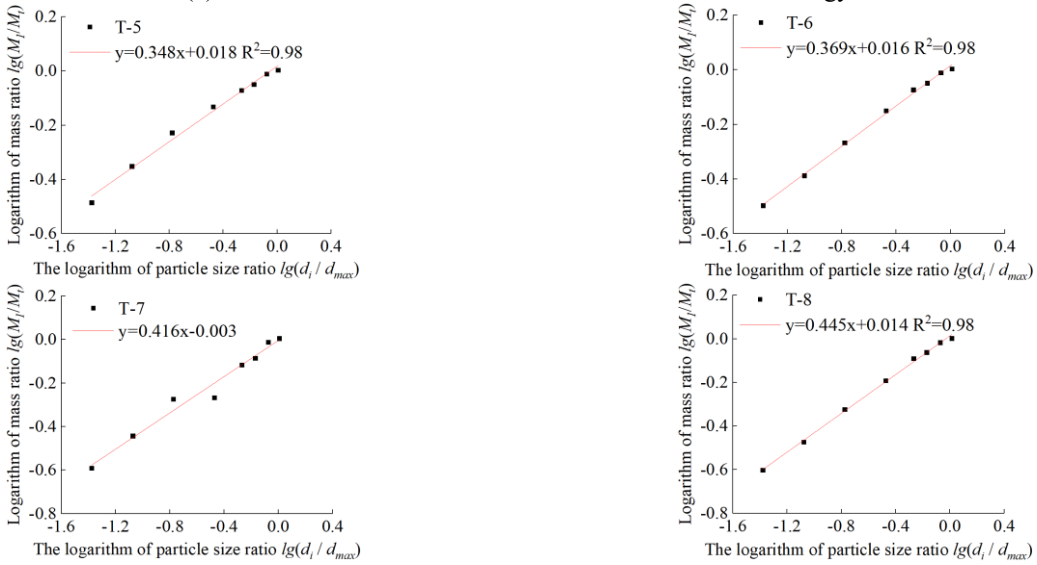

(b) Fractal dimension of voids under the influence of skeleton particle size distribution

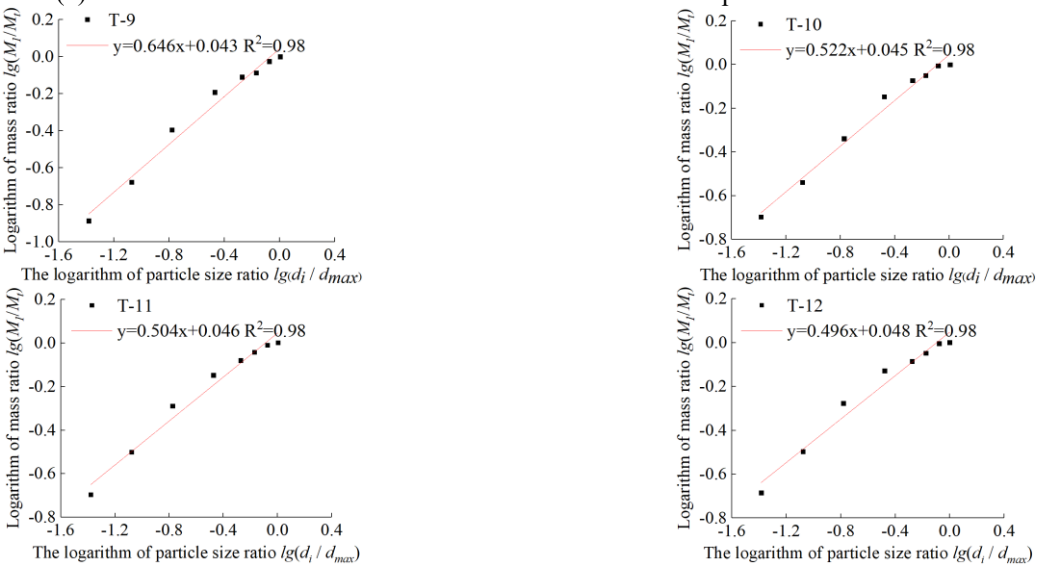

(c) Fractal dimension of voids under axial compression

Fig. 5 Void fractal dimension for each influencing factor

Additionally, as the axial stress increases, the fractal dimension of voids in broken rock samples gradually increases. Notably, when the axial stress is 5 MPa, 10 MPa, 15 MPa, and 20 MPa, the fractal dimensions of voids are 0.6457, 0.5222, 0.5044, and 0.4955, respectively. Consequently, it becomes evident that geological conditions characterized by harder lithology and shallower burial depth of the coal seam roof facilitate the formation of a larger number of voids with greater sizes, thereby enhancing the diffusion of gangue slurry.

4. Discussion

4.1 Relationship among void fraction, fractal dimension, and diffusion depth of gangue slurry

The diffusion of gangue slurry within the caving zone is intricately linked to the distribution of voids. By integrating the rheological parameters of gangue slurry, namely the consistency index C and power-law index n, with the void distribution parameters, including void fraction φ and void fractal dimension k, it is possible to accurately calculate the diffusion depth of the slurry. Gangue slurry, classified as a non-Newtonian power-law fluid, exhibits unique rheological properties. Given that the voids are typically curved, the flow rate of gangue slurry within them is calculated as demonstrated in Eq. (4).

$$q_{\mathrm{g}} = \pi\left(-\frac{1}{2C}\frac{dP}{dL_t}\right)^{1/n}\frac{n}{1+3n}r^{(1+3n)/n} \tag{4}$$

Where q_g represents the flow rate of gangue slurry within the void, C denotes the consistency index of gangue slurry, n signifies the power law index of gangue slurry, P stands for the grouting pressure, and L_t indicates the actual flow length of the slurry.

To better represent the diffusion depth of gangue slurry, the concept of apparent flow length (L_0) of gangue slurry is introduced, and its relationship with the actual flow length of the slurry is as follows

$$\mathrm{d}L_{\mathrm{t}}=L_0^{k-1}(2r)^{1-k}k\mathrm{d}L_0 \tag{5}$$

Where r is the radius of the void.

Upon further analysis, it can be deduced that the flow rate of gangue slurry passing through any given void is

$$q_g(r) = 2(k-1)/n\frac{n}{3n+1}\left(-\frac{1}{2C}\frac{\mathrm{d}P}{L_0^{k-1}k\mathrm{d}L_0}\right)^{1/n}r^{(k+3n)/n} \tag{6}$$

Integrating the above equation, we can obtain the total flow of all voids within the caving zone as follows

$$Q_g = \pi\frac{n^2}{3n+1}\left(-\frac{1}{2C}\frac{\mathrm{d}p}{\mathrm{d}L_0}\right)^{1/n}L_0^{(1-k)/n}k^{-1/n}2^{(k-1)/n}\frac{(3-k)\cdot r_{\max}^{\ 3+k/n}}{(1+n)k} \tag{7}$$

On any given section of the caving zone, the section area A can be calculated using the formula $A=A_p/\varphi$, where A_p represents the total area of voids and φ denotes the void fraction. Consequently, the formula for determining the section area of any region within the caving zone is as follows

$$\begin{cases} A_p = -\int_{r_{\min}}^{r_{\max}}\pi r^2 dN = \dfrac{\pi(3-k)}{k}r_{\max}^2[1-(\dfrac{r_{\min}}{r_{\max}})^k] \\ A = \dfrac{\pi(3-k)}{\phi k}r_{\max}^2[1-(\dfrac{r_{\min}}{r_{\max}})^k] \\ \phi = (\dfrac{r_{\min}}{r_{\max}})^k \end{cases} \tag{8}$$

Where r_{max} is the maximum size of the void and r_{min} is the minimum size of the void.

The average flow rate through cell section A is

$$V = \frac{Q_g}{A} \tag{9}$$

When the diffusion rate of gangue slurry reaches 0, the diffusion process ceases, and the apparent flow distance (L_0) of the gangue slurry at this point corresponds to its diffusion depth.

4.2 Gangue slurry diffusion depth evolution law

Using gangue as the aggregate and fly ash as the cementing material, a gangue slurry with a concentration of 70% is formulated. At this concentration, the slurry exhibits a consistency index (C) of 0.051 and a power law index (n) of 0.181. By incorporating the rheological parameters of the slurry and the void parameters of the collapse zone into Eqs. (1) to (4), we can derive the relationship between the diffusion rate and depth of the gangue slurry under various influencing factors, as illustrated in Fig. 6.

It can be deduced from Fig. 6 that the diffusion characteristics of gangue slurry are significantly influenced by the distribution patterns of voids within the caving zone. As the lithology of the rock blocks within the caving zone gradually softens, there is a notable decrease in the diffusion rate of gangue slurry, resulting in a gradual reduction in its diffusion depth. Specifically, when the lithology of the rock blocks comprises limestone, sandstone, mudstone, and shale, the diffusion depth of gangue slurry is observed to be 248, 216, 160, and 40 meters, respectively. Conversely, as the number of large-sized rock blocks increases within the caving zone, there is a marked increase in the diffusion rate of gangue slurry, leading to a gradual enhancement in its diffusion depth, ultimately reaching 136, 216, 264, and 272 meters, respectively. Furthermore, as axial stress increases, the diffusion rate of gangue slurry decreases significantly, causing a gradual decrease in its diffusion depth. For instance, when the axial stress levels are 5, 10, 15, and 20, the corresponding diffusion depths of gangue slurry are 272, 248, 224, and 192 meters, respectively.

In conclusion, the diffusion pattern of gangue slurry is intricately linked to the distribution of voids within the caving zone, with lithology exerting a significant influence on the extent of diffusion within this zone. Notably, a decrease in lithological hardness results in a substantial reduction in diffusion depth, reaching up to 208 meters.

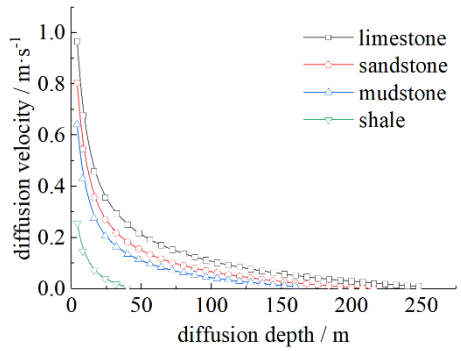

(a) Lithology

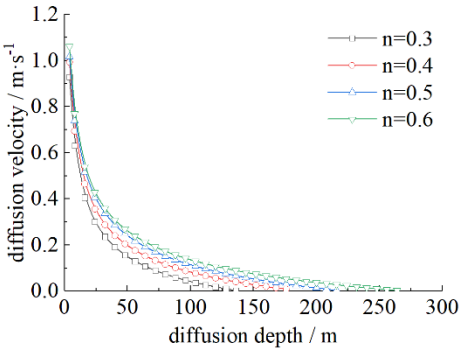

(b) Skeleton particle size distribution

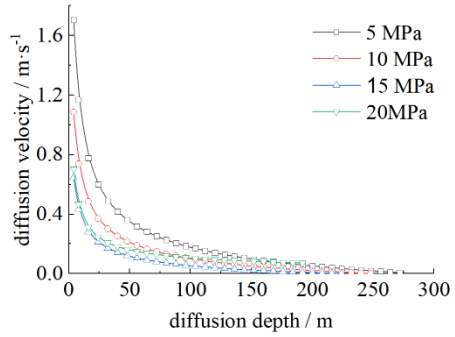

(c) Axial stress

Fig. 6 Diffusion depth of gangue slurry under different conditions

It is evident that lithology, skeleton particle grading, and axial stress are pivotal factors influencing the design of gangue slurry filling projects. Hard lithologies, such as limestone and sandstone, result in collapse zones with high porosity and fractal dimensions, substantially enhancing slurry diffusion depths (e.g., 248 m for limestone vs. 40 m for shale). Consequently, in such projects, it is crucial to optimize drilling spacing accordingly and prioritize filling in areas with hard roofs. The coarse particle grading of the skeleton impacts the porosity of the collapse zone, necessitating adjustments to the slurry aggregate particle size to enhance permeability. When necessary, segmented grouting techniques should be employed. Under conditions of low axial stress, the diffusion depth increases by 42% compared to high stress conditions (272 m vs. 192 m). Therefore, during design, preference should be given to shallow coal seams or timely filling post-mining to prevent void closure due to overlying rock compaction.

In practical engineering applications, efficient filling is achieved through the integration of dynamic monitoring and collaborative optimization. Loss of diffusion capacity can be compensated for by improving grading, while grouting pressure adjustments are made to overcome compaction resistance. By combining borehole sampling data (grading, porosity) from the collapse zone with real-time grouting data (pressure-flow curves), the slurry mix ratio and grouting parameters can be dynamically adjusted and refined.

4.3 Slurry diffusion engineering tests under typical geological conditions

(1) Overview of the filling area

Taking a mine in a mining area in Inner Mongolia as an experimental mine, a gangue grouting project was designed to fill gangue slurry into the caving zone in order to address the issues of gangue accumulation on the surface and ecological pollution in the surrounding mining area. The lithology of the fractured rock blocks within the caving zone primarily consists of coarse sandstone and medium sandstone. The coal seam has a mining thickness of 5 meters, and the caving zone extends over an area of 246 × 2775 × 60 meters with a buried depth of 660 meters. The designated filling timing is scheduled for after the complete extraction of the working face.

The coal seams in the filling area consist mainly of dull coal, with bright coal being the second most prevalent. The maximum mineable thickness of the coal seams is 6.4 m, the minimum is 5.4 m, and the average is 5.0 m, with virtually no interbedded shale. The immediate roof is predominantly composed of sandy mudstone (ranging from 0 to 4.97 m in thickness, with an average of 2.09 m) and siltstone (ranging from 0 to 11.3 m in thickness, with an average of 3.6 m). It has a compressive strength ranging from 31.68 to 32.3 MPa, with an average of 31.99 MPa, classifying it as a soft to semi-hard rock stratum. The main roof consists primarily of medium-grained gravel sandstone (ranging from 0 to 13.84 m in thickness, with an average of 5.695 m), coarse sandstone (ranging from 9.15 to 41.61 m in thickness, with an average of 25.85 m), and medium sandstone (ranging from 11.2 to 22.55 m in thickness, with an average of 16.36 m). It is dense and hard, with moderately developed fractures and well-developed bedding, exhibiting a massive structure. The compressive strength ranges from 15.2 to 19.08 MPa, with an average of 17.14 MPa, classifying it as a semi-hard rock stratum. The immediate floor is predominantly composed of siltstone and sandy mudstone, with a thickness ranging from 10.8 to 16.2 m and an average of 12.6 m. The bedding is well-developed, and it softens when exposed to water. The compressive strength ranges from 38.42 to 40.08 MPa, with an average of 39.25 MPa.

Based on field detection and calculations, the distribution of void fraction within the caving zone in this region exhibits the following characteristics: horizontally, the void fraction gradually decreases from 80% to 30% as one moves from the naturally accumulated area to the re-

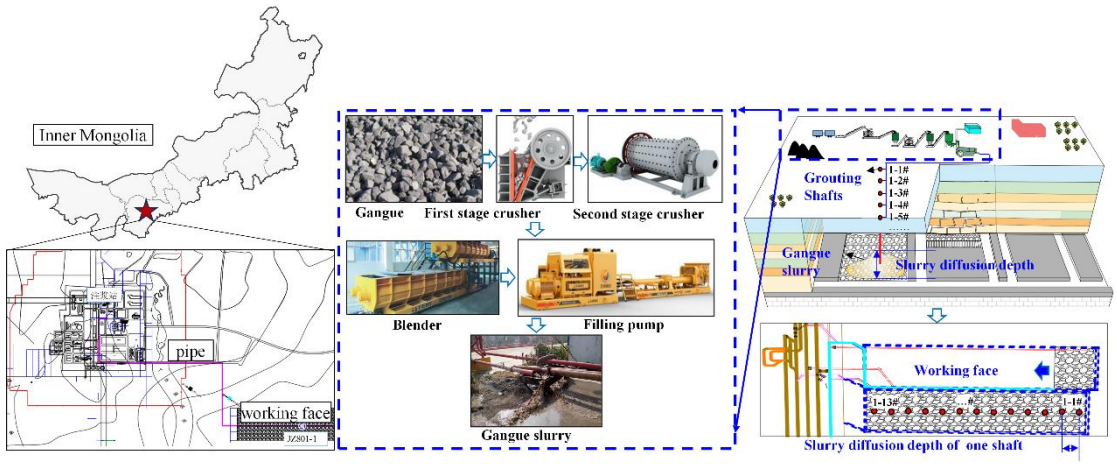

(a) Diagram of filling levels and filling equipment arrangement

(b) Gangue slurry at the site

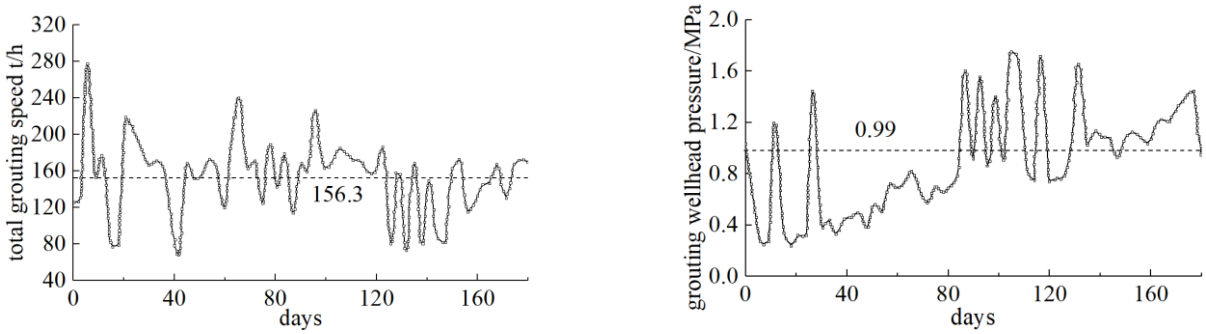

(c) Wellhead pressure and grouting speed

Fig. 7 Statistical chart of grouting wellhead pressure and grouting speed of gangue slurry

compacted area. Vertically, due to the natural accumulation state of the internally fractured rock masses, there is minimal variation in void fraction. Overall, the total volume of voids within the caving zone comprises approximately 38% of the extracted coal seam volume.

(2) Characteristics of the filling slurry

The designed gangue slurry is a mixture of gangue, fly ash, and water, with a concentration of 70%. Field testing has revealed a bulk density of 1.36 g/cm^3 for this slurry. Calculations indicate a diffusion depth of approximately 220 meters for the gangue slurry, thus justifying a layout spacing of 220 meters between adjacent shafts.

The designed gangue slurry consists of gangue, fly ash, and water, with a slurry concentration of 70%. Field tests have revealed a bulk density of 1.36 g/cm^3 for the gangue slurry and a density of 2.82 g/cm^3 for the gangue itself. The gangue slurry is classified as a power-law fluid, exhibiting a shear strength of 2.9 KPa, a sedimentation rate of 0.23, and a slump spread of 255 mm. When conveyed through a pipe with a diameter of $D133 \times 16$ mm, the Darcy friction factor is 0.00415.

The gangue slurry is prepared on the ground, and ground grouting shafts are arranged to facilitate the filling of the caving zone. Gangue slurry is prepared on the ground and the grouting shaft is arranged vertically. By analyzing the grouting effect of grouting shaft No. 3 during the grouting process, the layout and final grouting wellhead pressure and gangue slurry injection speed are depicted in Fig. 7.

(3) Actual measurements of slurry diffusion effects

Analysis of Fig. 7(c) reveals that the initial wellhead pressure required for grouting is relatively low. However, as

the slurry continues to be injected, the diffusion of the slurry gradually becomes more challenging, resulting in a gradual increase in wellhead pressure, ultimately stabilizing around 1.0 MPa. The average grouting speed in grouting shaft No. 3 attains 156.3 t/h, with an average grouting volume of 94,000 tons per month per hole. This translates to a slurry diffusion diameter of 220 meters per hole, which aligns with the theoretical analysis. Ultimately, the calculated average gangue disposal capacity per hole is 56,000 tons per month. By utilizing gangue slurry filling, the mine has successfully addressed the challenge of gangue disposal.

The aforementioned research findings indicate that to enhance the filling efficiency of gangue slurry, it is advisable to prioritize filling operations in mines with hard roof geological conditions, particularly those with limestone or sandstone roofs. Additionally, it is essential that the strata overlying the caving zone possess superior bearing capacity to prevent excessive axial pressure on the caving zone.

5. Conclusions

This paper aims to investigate the diffusion pattern of gangue slurry within the caving zone. Initially, a simulation test was conducted on the broken rock blocks within the caving zone to analyze the changes in the mass proportion of rock blocks of various particle sizes before and after bearing and crushing. Utilizing a bearing compression device, the evolution of void characteristics in the caving zone, influenced by lithology, skeleton particle size distribution, and axial stress, was examined. Furthermore, the diffusion pattern of gangue slurry was calculated based on a fluid force balance model tailored for gangue slurry diffusion. The conclusions were drawn:

- Based on the mining rock mass internal void evolution test system, we investigated the laws of lithology, skeleton particle gradation, and axial stress affecting the void ratio of the caving zone. Initially, rock samples with harder lithology and larger skeleton particles exhibited higher void fraction. However, as the lithology softened, the skeleton particle size decreased, and the axial stress increased, the void fraction in the caving zone gradually diminished, with maximum decreases reaching 0.3, 0.25, and 0.12, respectively. Evidently, lithology and skeleton particle size serve as the primary factors determining the evolution of void fraction.
- A statistical analysis was conducted on the gradation of skeleton particles with varying lithologies before and after crushing. The results indicate that particles sized 20~30 mm constitute the primary group susceptible to crushing, ultimately yielding 10~20 mm skeleton particles. Utilizing the Tyler fractal theory, the fractal dimension of voids within fractured rock blocks was computed. Notably, a harder lithology, larger coarse particle sizes within the skeleton, and lower axial stress correlate with a higher fractal dimension, suggestive of a greater number and size of voids within the fractured rock samples.
- Leveraging the fluid force balance model, the diffusion depth of gangue slurry within the caving zone was estimated. Incorporating the void fraction and fractal dimension data of fractured rock samples across various influencing factors, it was observed that lithology significantly impacts the diffusion depth within the caving zone. Specifically, a softening of the lithology led to a reduction in diffusion depth by 208 meters.
- Field measurements reveal that, when the roof of the caving zone comprises sandstone, the total volume of voids within the caving zone accounts for approximately 38% of the extracted coal seam volume. An analysis of grouting flow rates and wellhead pressure data indicates that the average velocity of gangue slurry can attain 156.9 tons per hour. Consequently, the estimated average grouting volume per shaft reaches 94,000 tons per month. The calculated diffusion diameter of the slurry through a single shaft is 220 meters, which aligns with the theoretical analysis findings.

Acknowledgements

This work was supported by the National Natural Science Foundation of China (52274135) and Major Technology Support Projects (BY2400007341).

References

Behera, B., Yadav, A., Singh, G.S.P. and Sharma, S.K. (2020), "Design of an optimum longwall face for improved ground control: a review", *J. Institution of Engineers (India): Series D*, **101**, 151-164. https://doi.org/10.1007/s40033-020-00216-3.

Feng, X., Wang, Y., Li, L., Jiang, Z., Zhou, G., Wu, Q. andWang, T. (2024), "Experimental investigation on physical properties and early-stage strength of ultrafine fly ash-based geopolymer grouting material", *Constr. Build. Mater*., **441**, 137526. https://doi.org/10.1016/j.conbuildmat.2024.137526.

Genis, M., Akcin, H., Aydan, O. and Bacak, G. (2018), "Investigation of possible causes of sinkhole incident at the Zonguldak Coal Basin, Turkey", *Geomech. Eng*., **16**(2), 177-185. https://doi.org/10.12989/gae.2018.16.2.177.

Gholizadeh, S., Leman, Z. and Baharudin, B.T.H.T. (2015), "A review of the application of acoustic emission technique in engineering", *Struct. Eng. Mech*., **54**(6), 1075-1095. https://doi.org/10.12989/sem.2015.54.6.1075.

Ghazifard, A., Moslehi, A., Safaei, H. and Roostaei, M. (2016), "Effects of groundwater withdrawal on land subsidence in Kashan Plain, Iran", *Bull. Eng. Geol. Environ*., **75**, 1157-1168. https://doi.org/10.1007/s10064-016-0885-3.

Hejmanowski, R. (2015), "Modeling of time dependent subsidence for coal and ore deposits", *Int. J. Coal Sci. Tech*., **2**, 287-292. https://doi.org/10.1007/s40789-015-0092-z.

Junker, M. and Witthaus, H. (2013), "Progress in the research and application of coal mining with stowing", *Int. J. Min. Sci. Tech*., **23**(1), 7-12. https://doi.org/10.1016/j.ijmst.2013.01.002.

Kamran, M., Shahani, N.M. and Armaghani, D.J. (2022), "Decision support system for underground coal pillar stability using unsupervised and supervised machine learning approaches", *Geomech. Eng*., **30**(2), 107-121. https://doi.org/10.12989/gae.2022.30.2.107.

Kostecki, T. and Spearing, A.J.S. (2015), "Influence of backfill on coal pillar strength and floor bearing capacity in weak floor conditions in the Illinois Basin", *Int. J. Rock Mech. Min. Sci*., **76**, 55-67. https://doi.org/10.1016/j.ijrmms.2014.11.011.

Kim, S.M., Suh, J., Oh, S., Son, J., Hyun, C.U., Park, H.D., Shin,

S.H. and Choi, Y. (2016), "Assessing and prioritizing environmental hazards associated with abandoned mines in Gangwon-do, South Korea: The total mine hazards index", *Environ. Earth Sci.*, **75**, 1-14. https://doi.org/10.1007/s12665-016-5283-4.

Li, X., Chen, S., Zhang, Q., Gao, X. and Feng, F. (2021), "Research on theory, simulation and measurement of stress behavior under regenerated roof condition", Geomech. Eng., **26**(1), 49-61. https://doi.org/10.12989/gae.2021.26.1.049.

Lou, Z., Wang, K., Zhao, W., Wei, G., Yao, H., Qin, H., Wei, X. and Song, H. (2024), "Experimental investigation on visualization and quantitative characterization of filling and plugging performances of fractures in coal", *Phys. Fluids*, **36**(3). https://doi.org/10.1063/5.0200165.

Li, H., Zha, J., Zhang, H., Zheng, N. and Guo, G. (2020), "Design method for cadmium and arsenic contamination control during the mining-selecting-backfilling integrated technology", *J. Cleaner Product.*, **261**, 121259. https://doi.org/10.1016/j.jclepro.2020.121259.

Liu, F., Silva, J., Yang, S., Lv, H. and Zhang, J. (2019), "Influence of explosives distribution on coal fragmentation in top-coal caving mining", *Geomech. Eng.*, **18**(2), 111-119. https://doi.org/10.12989/gae.2019.18.2.111.

Mohammadi, S., Ataei, M. and Kakaie, R. (2018), "Assessment of the importance of parameters affecting roof strata cavability in mechanized longwall mining", *Geotech. Geol. Eng.*, **36**, 2667-2682. https://doi.org/10.1007/s10706-018-0490-2.

Mondal, D., Roy, P.N.S. and Behera, P.K. (2017), "Use of correlation fractal dimension signatures for understanding the overlying strata dynamics in longwall coal mines", *Int. J. Rock Mech. Min. Sci.*, **91**, 210-221. https://doi.org/10.1016/j.ijrmms.2016.11.019.

Mo, S., Canbulat, I., Zhang, C., Oh, J., Shen, B. and Hagan, P. (2018), "Numerical investigation into the effect of backfilling on coal pillar strength in highwall mining", *Int. J. Min. Sci. Tech.*, **28**(2), 281-286. https://doi.org/10.1016/j.ijmst.2017.07.003.

Mishra, D.P., Panigrahi, D.C., Kumar, P., Kumar, A. and Sinha, P.K. (2021), "Assessment of relative impacts of various geo-mining factors on methane dispersion for safety in gassy underground coal mines: an artificial neural networks approach", *Neural Comput. Appl.*, **33**(1), 181-190. https://doi.org/10.1007/s00521-020-04974-9.

Prendes-Gero, M.B., Alcalde-Gonzalo, J., Ramírez-Oyanguren, P., Suárez-Domínguez, F.J. and Álvarez-Fernández, M.I. (2013), "Longwall mining stability in take-off phase", *J. Appl. Math.*, **2013**(1), 859803. https://doi.org/10.1155/2013/859803.

Roy, R., Chakraborty, S., Bisai, R., Pal, S.K. and Mishra, S. (2023), "Gravity blind backfilling of abandoned underground mine voids using suitable mix proportion of fill materials and method of filling", *Geotech. Geol. Eng.*, **41**(3), 1801-1819. https://doi.org/10.1007/s10706-022-02371-8.

Singh, G.S.P. and Singh, U.K. (2010), "Numerical modeling study of the effect of some critical parameters on caving behavior of strata and support performance in a longwall working", *Rock Mech. Rock Eng.*, **43**, 475-489. https://doi.org/10.1007/s00603-009-0061-1.

Sharma, P., Mahure, N.V. and Ratnam, M. (2011), "Influence of different stress conditions on behavior of rockfill materials", *Geotech. Geol. Eng.*, **29**, 1035-1048. https://doi.org/10.1007/s10706-011-9435-8.

Song, M.K., Kim, S.H. and Choi, C.K. (2006), "Enhanced finite element modeling for geometric non-linear analysis of cable-supported structures", *Struct. Eng. Mech.*, **22**(5), 575-598. https://doi.org/10.12989/sem.2006.22.5.575.

Van Dyke, M.A., Su, W.H. and Wickline, J. (2018), "Evaluation of seismic potential in a longwall mine with massive sandstone roof under deep overburden", *Int. J. Min. Sci. Tech.*, **28**(1), 115-119. https://doi.org/10.1016/j.ijmst.2017.12.014.

Verma, A.K., Kishore, K. and Chatterjee, S. (2016), "Prediction model of longwall powered support capacity using field monitored data of a longwall panel and uncertainty-based neural network", *Geotech. Geol. Eng.*, **34**, 2033-2052. https://doi.org/10.1007/s10706-016-0081-z.

Wesseloo, J. (2018), "The spatial assessment of the current seismic hazard state for hard rock underground mines", *Rock Mech. Rock Eng.*, **51**(6), 1839-1862. https://doi.org/10.1007/s00603-018-1430-4.

Xue, D., Hu, X., Faradonbeh, R.S., Fang, H. and Chang, P. (2024), "CFD characterization and field test study on plugging air leakage with time-varying viscosity solidified foam to prevent coal spontaneous combustion", *Combust. Sci. Technol.*, 1-31. https://doi.org/10.1080/00102202.2024.2358988.

Yin, W., Miao, X., Zhang, J. and Zhong, S. (2017), "Mechanical analysis of effective pressure relief protection range of upper protective seam mining", *Int. J. Min. Sci. Tech.*, **27**(3), 537-543. https://doi.org/10.1016/j.ijmst.2017.03.021.

Yoon, S., Kim, D.M., Yu, S., Batsaikhan, B., Kim, T. and Yun, S.T. (2024), "Characteristics of soil contamination by potentially toxic elements in mine areas of Mongolia", *Environ. Geochem. Health*, **46**(1), 15. https://doi.org/10.1007/s10653-023-01812-4.

Zhang, J., Li, B., Zhou, N. and Zhang, Q. (2016), "Application of solid backfilling to reduce hard-roof caving and longwall coal face burst potential", *Int. J. Rock Mech. Min. Sci.*, **88**, 197-205. https://doi.org/10.1016/j.ijrmms.2016.07.025.

Zhang, Q., Du, C.L., Zhang, J.X., Wang, J.Q., Li, M. and Qi, W.Y. (2018), "Backfill support's backfill and operation properties and evaluation", *J. Central South Univ.*, **25**(6), 1524-1534. https://doi.org/10.1007/s11771-018-3845-1.

GC